ADVANCED MATERIALS
www.advmat.de

Probing Electronic Band Structures of Dielectric Polymers via Pre-Breakdown Conduction

Zongze Li, Chao Wu, Lihua Chen, Yifei Wang, Zeynep Mutulu, Hiroaki Uehara, Jierui Zhou, Miko Cakmak, Rampi Ramprasad, and Yang Cao**

The electronic band structure, especially the defect states at the conduction band tail, dominates electron transport and electrical degradation of a dielectric material under an extremely high electric field. However, the electronic band structure in a dielectric is barely well studied due to experimental challenges in detecting the electrical conduction to an extremely high electric field, i.e., prebreakdown. In this work, the electronic band structure of polymer dielectric films is probed through an in situ prebreakdown conduction measurement method in conjunction with a space-charge-limited-current spectroscopic analysis. An exponential distribution of defect states at the conduction band tail with varying trap levels is observed in accordance with the specific morphological disorder in the polymer dielectric, and the experimental defect states show also a favorable agreement with the calculated density of states from the density functional theory. The methodology demonstrated in this work bridges the molecule-structure-determined electronic band structure and the macro electrical conduction behavior with a highly improved understanding of material properties that control the electrical breakdown, and paves a way for guiding the modification of existing material and the exploration of novel materials for high electric field applications.

1. Introduction

Polymer dielectrics are among the most pervasive and critical materials used as electrical insulation and electrostatic energy storage in electrical and electronic systems.[1–5] The ever-increasing need for payload efficiency and long-term operational stability calls for polymer dielectrics operable at a higher electric field. Dielectric degradation, which eventually culminates in the breakdown, is extremely complex, involving the conformational and electronic features of polymers, multi-factor interactions from electrical, thermal, mechanical, and chemical properties. The complexity of these processes makes the breakdown mechanism far from fully understood despite extensive effort over almost the past century.[6,7]

Of particular significance is to experimentally investigate the physical nature of charge transport and probe the fundamental parameters of electronic band structures that are related to dielectric degradation and breakdown when subjected to extremely high electric fields.[8–12] The intrinsic breakdown strength of a material is related to its band gap value, and a material with a larger band gap usually will display a higher threshold for impact ionization.[13,14] However, unlike an ideal crystalline material with a clean band gap, polymers exhibit physical disorders due to long-chain folding and weak inter-chain interactions, which lead to defect state creation in the forbidden band and band edge shifting.[15] The defect states in polymers directly interact with carriers and shift the electrical conduction band edge, promoting charge transport and leading to dielectric breakdown.[16]

Z. Li, C. Wu, Y. Wang, J. Zhou, Y. Cao
Electrical Insulation Research Center
University of Connecticut
97 N Eagleville Rd, Storrs, CT 06269, USA
E-mail: wuchaothu@tsinghua.edu.cn; yang.cao@uconn.edu
Z. Li, C. Wu, Y. Wang, J. Zhou, Y. Cao
Electrical and Computer Engineering
University of Connecticut
371 Fairfield Way, Storrs, CT 06269, USA
C. Wu
Department of Electrical Engineering
Tsinghua University
Beijing 100084, China
L. Chen, R. Ramprasad
School of Materials Science and Engineering
Georgia Institute of Technology
771 Ferst Drive NW, Atlanta, GA 30332, USA
Z. Mutulu, M. Cakmak
Departments of Materials Engineering and Mechanical Engineering
Purdue University
West Lafayette, IN 47907, USA
H. Uehara
Department of Electrical Engineering
Kanto Gakuin University
1-50-1 Mutsuura-higashi, Kanazawa-ku, Yokohama 236–8501, Japan

The ORCID identification number(s) for the author(s) of this article can be found under https://doi.org/10.1002/adma.202310497

DOI: 10.1002/adma.202310497

The electronic band structures and defect states in polymer dielectrics have only been characterized by quasi-steady state electrical conduction measurement,[17] thermoluminescence,[18] thermal stimulated current measurement[19] or optical measurement, which were all performed under relatively low or without electric fields.[20] Dielectric breakdown happens when a conduction current flows through an insulating dielectric uncontrollably, thus, electric conduction is closely related to the band-structure-controlled breakdown phenomenon. Among the aforementioned characterizations, electrical conduction measurement provides the most direct information on band structures and defect states correlated to charge transport and electrical breakdown. Electrical conduction in insulating materials is dependent on the applied electric fields. At a higher electric field, the band structure will be tilted severely by the applied field, giving electrons a higher possibility of entering the conduction band.[21] At extremely high fields, the conduction current is then generally dominated by trap-controlled conduction or band conduction (**Scheme 1**). The creation of charges with high mobility and the resulting rapid aging and catastrophic failure of dielectrics only happen at the electric field just before breakdown, a stage called the "prebreakdown".[22] Thus, electronic band structure derived from high field prebreakdown conduction will provide direct insight into electrical conduction and breakdown mechanism in wide band polymer dielectrics.[23] Therefore, electrical conduction at the pre-breakdown fields was desired to obtain the electronic band information that controls the breakdown of a dielectric.

However, prebreakdown conduction measurement in solid dielectrics remains challenging compared with that in semiconductors or other materials. The transient measurement of the conduction current will result in the capacitive absorption current that is much larger than the conduction current. Currently, no existing experimental method can properly characterize the prebreakdown conduction current in polymer dielectric thin films. The widely used conduction measurement in insulators is based on quasi-steady-state current measurement which could only reach around two-thirds of the breakdown field due to thermal breakdown caused by thermal runaway.[24] At these relatively low electric fields, electrons are more likely to transport by tunneling or hopping effect without entering the conduction band.[17] Researchers tried other methods such as high-temperature measurement, which can only be applied to a few heat-resistant polymers with compromised accuracy.[25] As can be expected, a novel method that can measure the prebreakdown conduction through polymer dielectrics, and a generic method that can reveal the defect states that control the electrical conduction, are urgently needed.

In this study, we fill this gap by probing the trap density of states (DOS) in polymers based on a prebreakdown conduction measurement and a modified temperature-dependent (TD) space-charge-limited-current (SCLC) spectroscopy. Prebreakdown conduction through polymer films is characterized by a specially designed novel measurement system to make information regarding trap-modulated conduction available for the first time. Based on the experimental prebreakdown conduction results, the defect DOS at the conduction band edge is calculated using a modified TD-SCLC theory. Favorable agreement with density functional theory (DFT) simulation results suggests that the measured defect density of states depends on the regularity of the polymer structure. This work ultimately contributes toward the fundamental understanding and detection of charge transport-related electronic band structure of polymer dielectrics, with the promise of revealing the essential correlation between electronic band structure and dielectric breakdown.

2. Results

2.1. Prebreakdown Conduction

Given the unavoidable challenge in steady-state measurements, the prebreakdown field in polymer films can only be reached under a transient condition during a high-voltage ramp. Under the transient condition, the measured total current through the film is a combination of the capacitive and conduction current, that is, $j(t) = \varepsilon_0 \varepsilon_r (\partial E(t))/\partial t + j_\sigma(t)$, where $j(t)$ is the measured current, ε_0 the vacuum permittivity, ε_r the relative permittivity, $E(t)$ the applied electric field, $j_\sigma(t)$ the conduction current and t the time. For capacitors in transient conditions, the magnitude of the capacitive current can be orders higher than the conduction current. Thus, to measure the prebreakdown conduction in real-time, the large capacitive current needs to be removed from the measured total current. This is achieved by a specially designed system based on active feedback control to cancel the capacitive current and reveal the prebreakdown conduction (see Experimental Section).[26] Based on the novel measurement system, prebreakdown conduction was measured in four typical polymer dielectric films with capacitor-grade to minimize variables, and the films investigated were draft-tender bi-axially oriented polypropylene (tender BOPP), simultaneous blow-molding bubble BOPP, polyethylene terephthalate (PET), and polystyrene (PS).

The measured integrated conduction current (charge) as a function of the electric field for the above polymers is shown in **Figure 1a**. For ease of observation, the result was replotted in Figure S1 (Supporting Information) with current density (j) versus electric field (E) consistent with standard analysis. The charge (Q) field (E) curves are found to have distinct characteristics at low and high electric fields (separated at ~300 MV m^{-1}). At a low electric field, all measured curves are straight lines with negligible slopes following Ohm's law, which is typically found in insulating dielectrics. At a high electric field, the measured conduction starts to grow nonlinearly, reaching a significant value before breakdown. This exponential increase of conduction could lead to damage to the chemical bindings and physical morphology within polymers.[27]

Among the films studied, the state-of-art capacitor film, semicrystalline tender BOPP with the highest dielectric breakdown strength of 771 kV mm^{-1} (Figure S2, Supporting Information), exhibits the lowest magnitude of conduction (1 μC). In comparison, the amorphous PS with the lowest dielectric breakdown strength of 444 kV mm^{-1} shows an order of magnitude higher conduction (15 μC). Bubble BOPP is found to have slightly higher conduction than tender BOPP and PET is found to be in between BOPP and PS. The measurement results on prebreakdown conduction correlate well with their dielectric performance and provide quantitative information for better separation/classification of different polymers than traditional electrical conduction

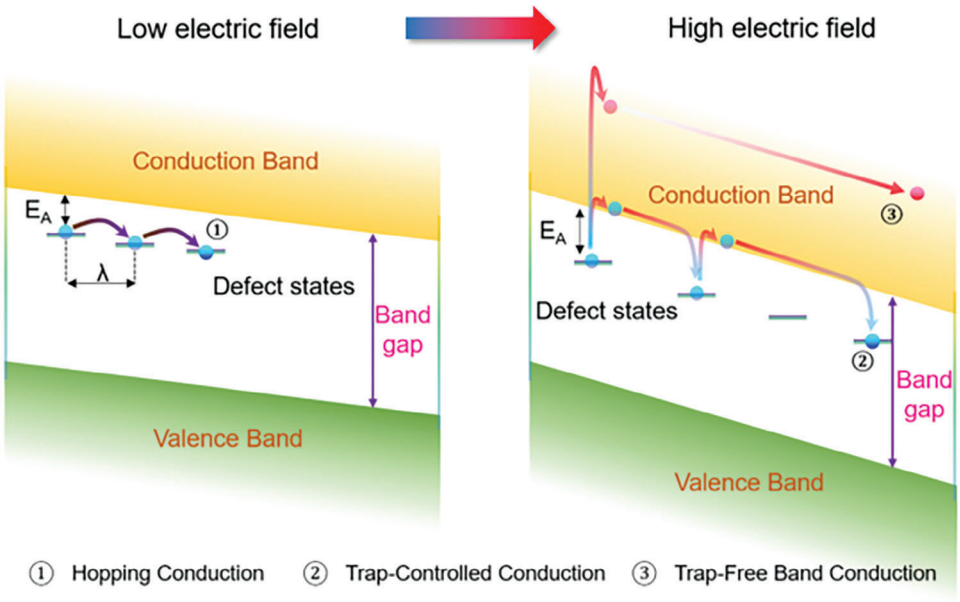

Scheme 1. Electronic band structure under low and high electric fields and related conduction theories.

measurements carried out at relatively low fields or based only on DC breakdown measurement.

The conduction current as a function of the electric field can be further analyzed with the Space-Charge-Limitted-Current (SCLC) conduction model to probe the electronic band structure of dielectrics.[28] For a realistic engineering dielectric with localized traps, there will be four regions for the applied field versus charge (integrated conduction): Ohmic region ($Q \propto E^2$), trap-modulated SCLC region ($Q \propto E^3$), trap-filled limited region ($Q \propto E^n$) and trap free region ($Q \propto E^3$). The integrated conduction versus electric field result is plotted under the logarithm scale in Figure 1b according to the SCLC model. The results measured below 300 MV m^{-1} is not used due to the low signal-to-noise ratio. At high fields above 300 MV m^{-1}, all Q–E curves start with a slope of 3, showing the trap-modulated conduction behavior. All the materials exhibited trap-filled limited conduction beyond a certain electric field with slopes higher than 3, indicating the dominant role of defect trap states over the conduction and charge transport at a high field.[29] The transition from trap-limited to trap-filled-limited region is not sharp, indicating a wide distribution in the energy of localized traps.

2.2. Localized Defect Density of States

Since the prebreakdown conduction is controlled by the defect states, quantitative analysis based on high filed conduction theory is utilized to probe the electronic band structure. The analysis is based on a modified temperature dependent SCLC (TD-SCLC) spectroscopic analysis adopted from the semi-conductor field. According to the TD-SCLC theory described by Schauer,[30] the shape of these experimentally determined SCLC curves reflects the increment of the excess charge relative to the shift of Fermi energy during the high voltage ramp. The first and

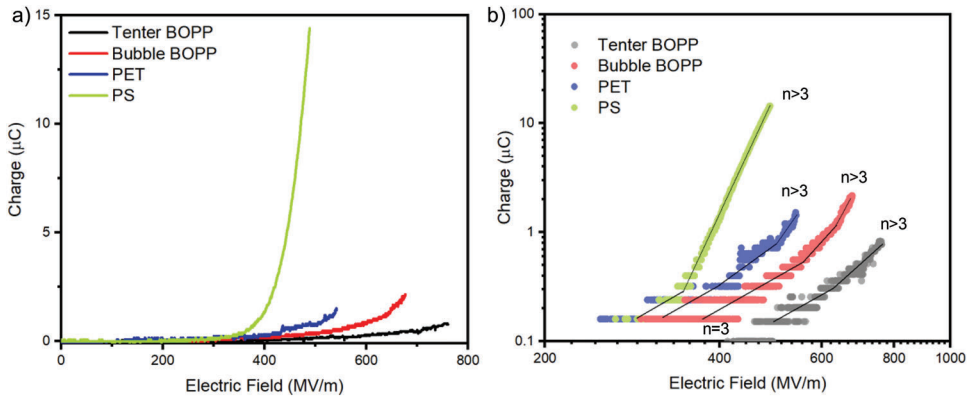

Figure 1. Prebreakdown conduction in polymer dielectric films. a) The integrated conduction for the four capacitor-grade films up to the prebreakdown field. b) Prebreakdown conduction under logarithm scale according to the SCLC model with the solid line showing the slope of the integrated conduction. The slope of larger than 2 + 1 indicates the presence of traps.

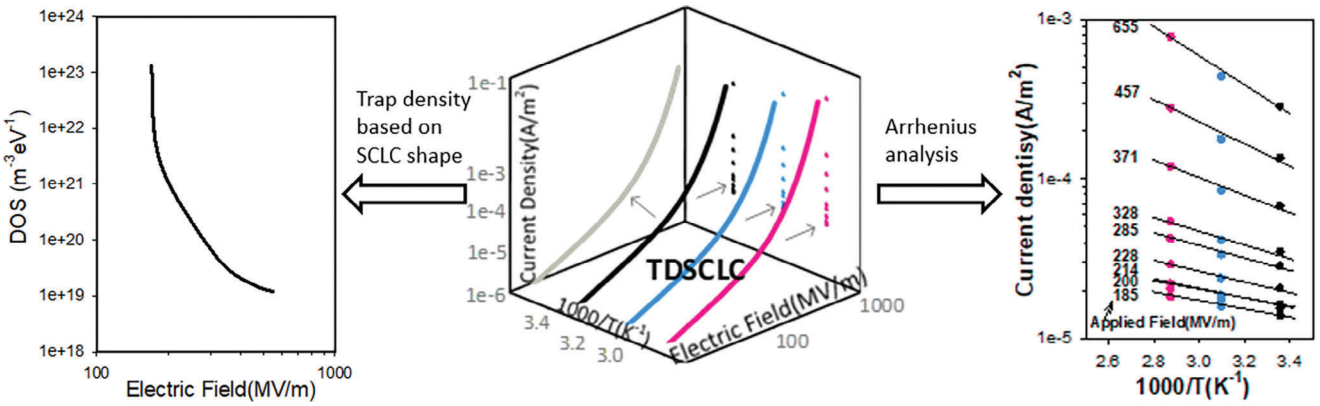

Figure 2. Data processing schematic for the extraction of defect DOS. The density of state information is extracted from the left projection and the activation energy is extracted from the right projection, and the reconstruction of the density of the trap state is achieved by combining the field-dependent DOS with field-dependent activation energies.

higher-order derivatives of the temperature-modulated current density plots with respect to the electric field (dj/dU and d^2j/dU^2) can be employed to yield transport parameters such as defect density of states (DOS).[31] For a simplified transport model with unipolar carrier injection from an ideal ohmic contact, the application of the SCLC analysis to the coupled transport and Poisson equations can derive the bulk defect DOS, measured in reference to the mobility edge of the conduction band. For the complete reconstruction of the defect DOS, Arrhenius analysis is also performed. This analysis method enables the determination of the density of electron localized states from prebreakdown conduction results in polymer dielectrics.

The TD-SCLC method is illustrated in **Figure 2**. The 3D data plot is the experimental TD-SCLC results of tender BOPP up to 700 MV m^{-1} under 25, 50, and 70 °C. Current density is obtained by taking derivatives of the measured charge with respect to time. Trap density is calculated as a function of the applied electric field based on the shape of the SCLC curve using the principle described above, with governing equations given in the Experimental Section. Current density as a function of temperature is used to calculate the trap depth as a function of the electric field. Combining the information from the previous two parts, the bulk trap DOS can be obtained.

The bulk trap DOS with respect to the conduction band edge are shown in the insert of **Figure 3**. Note that the amorphous PS shows a much higher conduction, indicating a different conduction mechanism in comparison to the other 3 semi-crystalline materials.

An exponential distribution of bulk trap DOS is observed for all three semi-crystalline materials, with the trap density ranging from 10^{19} to 10^{24} m^{-3} eV^{-1} at the conduction band edge. All three semi-crystalline materials show decreased density toward deeper traps. As for the trap depth, PET shows the shallowest defect level (0.2–0.4 eV), the state-of-art tender BOPP has a slightly deeper trap depth (0.3–0.5 eV) followed by bubble BOPP (0.5–0.7 eV). It is noteworthy that tender BOPP and bubble BOPP with the same chemical structure show distinct defect DOS distributions. The result indicates clearly that this method can probe the distinctive defect DOS due to different levels of physical disorder among polymers even with the same chemical structure.

The measured defect DOS results unraveled the impacts of physical morphology on the electronic band structures. For BOPP and PET, trap depths of less than 1 eV are observed, indicating that the trapping/de-trapping process or trapping-controlled conduction is favored.[32] The result also suggests that semi-crystalline polymers usually are promising candidates with lower electrical conduction and higher breakdown strength.

2.3. The Origin of the Measured Defect DOS

To further characterize the origins of the physical experimental results, the total DOS of crystal and amorphous phases of isotactic PP and PET were computed using the hybrid DFT method (see Experimental Section) and the results are shown in Figure 3. The DFT model on a smaller scale with two extreme phases of polymers are simulated, that is, pure crystalline phase and pure amorphous phases. The DFT model on a smaller scale with two extreme phases of polymers are simulated, that is, pure crystalline phase and pure amorphous phases. The band gap refers to the conduction and valence band edges difference in the crystal region. The difference between the states of crystalline and amorphous regions at conduction band edges presents the depth of electron traps formed due to the physical disorder at amorphous regions of semicrystalline polymers. The actual electron trap depth is dependent on the morphologic properties of the material such as the crystallinity. Note that the simulation is generated arbitrarily which may not fully reflect the exactly same situation in the tested polymers. Both the trap depth level and the DOS distribution of amorphous PS are very different from semi-crystalline materials. PS with very high magnitude and slope of conduction may follow another conduction mechanism that does meet the assumption of TD-SCLC analysis. It is possible that the highly disordered structure of PS with complete amorphous features (Figure S3, Supporting Information) leads to the tunneling of charges through the imperfect interface regions of PS and the metal electrodes. The effect of complete amorphous nature of PS on charge injection at electrode–polymer interface and transport, via c.a. the electron–phonon scattering, will need further study.

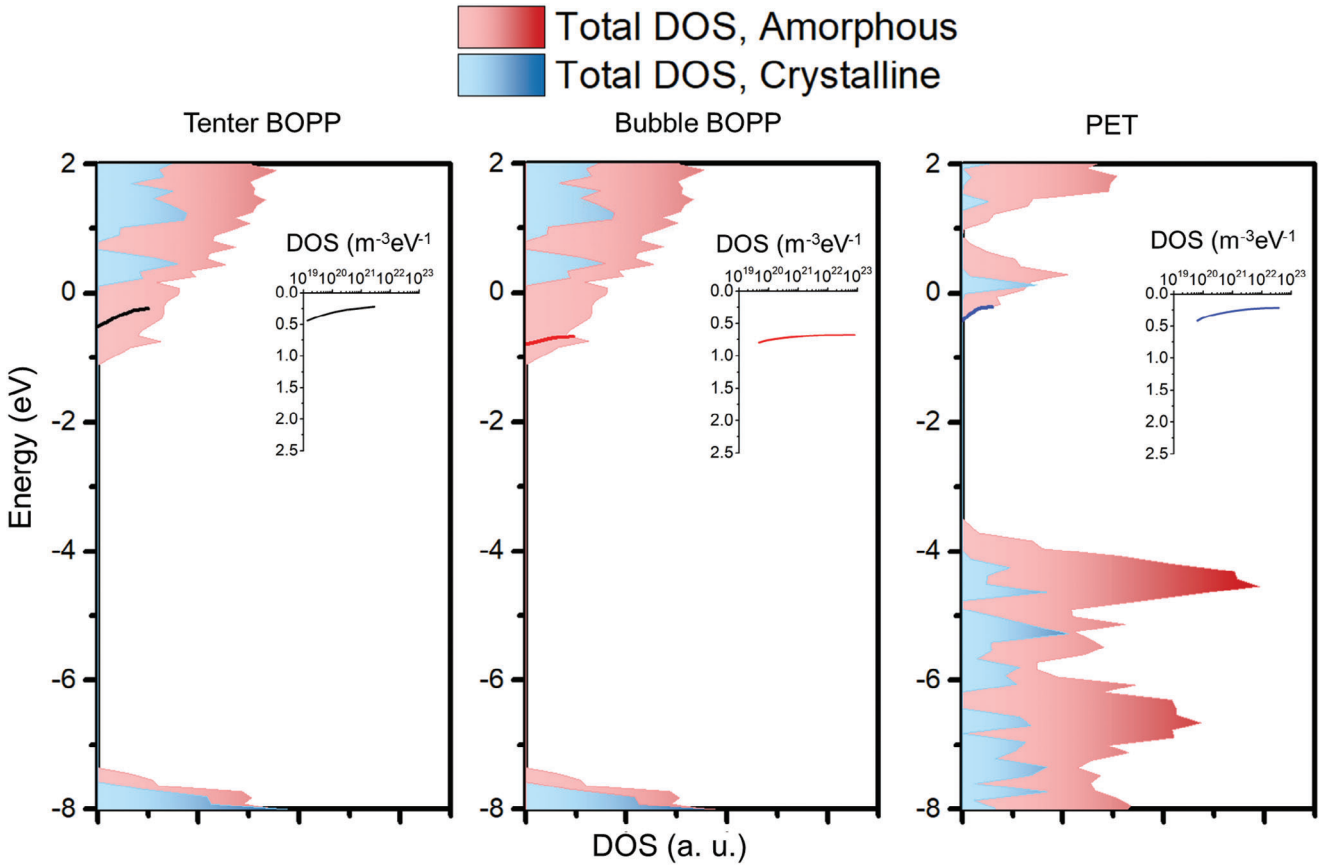

Figure 3. The total DOS of crystalline and amorphous phases in polymers based on first principle DFT simulation, as well as the experimentally calculated bulk trap DOS below the conduction band edge. The inserted plot shows the calculated value of trap DOS with original units and the main plot uses arbitrary units in accordance with DFT simulation.

The electron trap depth of tender PET (0.2–0.4 eV) is lower than that of tender PP (0.3–0.5 eV). This is caused by the low density of amorphous phases in PET, which reduces the overlaps of anti-bonding orbitals. To better understand the electronic band structure of these polymers, the experimental results are also included in Figure 3 with the arbitrary unit of trap density. The experimentally derived DOS correlates well to the first principles computation for all three semi-crystalline materials. Even the shape of measured DOS edges (i.e., band tails) matches well with that of the computed results at specific density peaks.

The origin of the measured DOS can be explained by the distinct morphological disorder states of all crystalline films. Materials characterization and analysis including wide-angle X-ray scattering (WAXS, Table S2, Supporting Information) and small-angle X-ray scattering (SAXS, Figure S4, Supporting Information) are performed to provide more detailed morphological information for all crystalline films. The WAXS patterns and spectra are shown in **Figure 4**, where both types of BOPP and PET are all found to be roughly equal biaxially oriented with a slight bias toward the transverse direction. The WAXS patterns with X-ray taken in ND (first row in Figure 4a) indicate that crystalline diffraction peaks are nearly random distribution in the film plane, that is, in-plane isotropy, for all crystalline films. Extremely high orientation of crystalline domains in both BOPP and PET are clearly evidenced in WAXS patterns taken in TD (the second row in Figure 4a). To examine the crystallite sizes in crystalline domains, we did peak separation of diffraction profiles for BOPP and PET films and determined the crystal sizes in selected crystallographic directions (Figure 4b, Table S2, Supporting Information). As it can be observed the crystal sizes in both BOPP films are much larger than those exhibited by PET. It is also interesting to note that tender BOPP exhibits larger crystal sizes in all respective crystallographic directions normal to (110), (040) (130) as compared to bubble BOPP. Within the resolution of the SAXS camera, we can measure long periods of Bubble BOPP (27.3 nm) and PET (14.2 nm). The line profile for Tender BOPP suggests there is a shoulder at a smaller Q, suggesting that the long period for Tender BOPP is larger than Bubble BOPP (Figure S5, Supporting Information).

Tender BOPP films are formed by extrusion through a heated slot die, cooling, reheating, and sequential stretching to induce machine-direction-orientation and transverse-direction-orientation for the formation of extended lamellar structures in monoclinic form.[33] On the other hand, bubble BOPP films are made with simultaneous bi-axial drawing from a tubular stalk. Upon reheating the exterior spherulites undergo a phase transition from hexagonal to dense monoclinic form.[34] Tender BOPP is found to have better biaxial orientation versus bubble

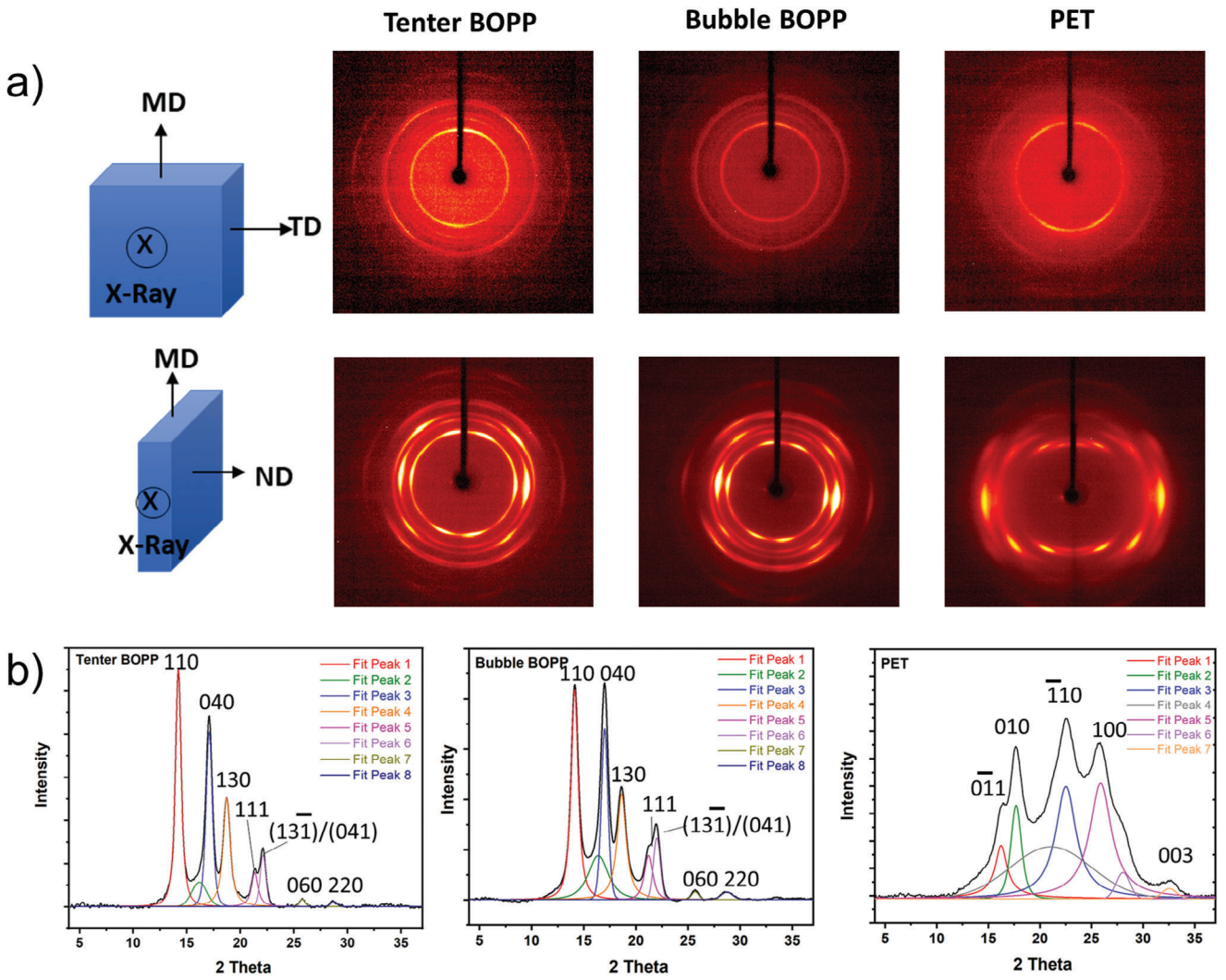

Figure 4. Materials characterization of three semi-crystalline polymers to show the origin of the defect states. a) WAXS patterns from normal direction and transverse direction. b) WAXS spectra from the transverse direction for showing the crystalline phase peaks.

BOPP from its clearer two-directional patterns from the Crossed Polarized-light Microscopy characterizations (Figure S3, Supporting Information). Tender BOPP film also exhibits slightly higher crystallinity (58%) as compared to bubble BOPP (54%), indicating the more ordered morphological features (Figure S7, Supporting Information). The different defect DOS in two BOPP films shows that the prebreakdown measurement can reflect the difference in the realistic morphological states of the polymer. Tender BOPP with higher crystallinity and larger crystallite sizes indicates better chain orientation due to stretching, contributing to shallower trap depth (closer to the total DOS of crystalline structure) when compared with bubble BOPP. At the same time, PET with a lower crystallinity demonstrates a trap depth very close to the total DOS of the amorphous structure. This important information can be used to optimize the manufacturing process of existing polymer dielectrics.

It is also noted that the defect levels of tender BOPP and PET are very similar, but PET exhibits higher conduction and lower breakdown strength. This is because BOPP has a wide band gap of 7 eV, while PET has a small band gap value of 4 eV. It can be seen from Figure 3 that the valence band maximum value of PET is much higher than that of BOPP, indicating the interband impact ionization is more appreciable in PET, resulting in a low breakdown strength. The electronic band gap originating from the ideal structure and the defect DOS originating from the realistic morphological states concurrently determine the prebreakdown conduction and breakdown in polymer dielectrics.

3. Conclusion

The current work proposes an effective approach that can successfully probe the defect DOS at the conduction band edge of polymer dielectrics by using the TD-SCLC analysis on prebreakdown conduction results, thus bridging the electronic band structure with the micro-structure in dielectrics. Pre-breakdown conduction was measured with the help of a specially designed capacitive current cancellation system. The pre-breakdown conduction measurement provides the most relevant information

related to electronic band structures, indicating the conduction is controlled by defect states. The reconstruction of defect DOS provides a quantitative basis f determining charge traps that dominate charge transport and breakdown of polymer dielectrics. The experimental results compare favorably with the DFT simulation, showing that the electrical properties of polymers are fundamentally related to their electronic band structures. Moreover, this work establishes the correlation between electrical conduction and polymer macromolecular structure. This is a novel and universal method that can be employed to experimentally probe the defect states in polymer dielectric films, which contributes toward the fundamental understanding of charge transport-related prebreakdown conduction and dielectric breakdown. The method in this work can also be used for screening novel dielectrics and for diagnosing high-field aging of dielectrics.

4. Experimental Section

Materials: Four types of capacitor-grade films were included in this study. They were 7.6 µm bi-axially oriented polypropylene (BOPP) film manufactured by the sequential draft-tender process from Bolloré, 12.5 µm BOPP film manufactured by the simultaneous-stretching process (bubble/blow-molding), 11.5 µm polyethylene terephthalate (PET) film manufactured by blade casting method, and 10 µm polystyrene (PS) film made through stretching method. All the materials under study possessed stereoregularity.

Material characterization results including WAXS, SAXS (Figures S4,S5, Supporting Information), 3D surface profilometer (Figure S6, Supporting Information), yielded that tender BOPP, bubble BOPP, and PET were semi-crystalline films while PS was completely amorphous. The differential scanning calorimetry (DSC) measurement confirmed the crystallinity of the three semi-crystalline films (Figure S7, Supporting Information). WAXS patterns indicated that tender BOPP had better bi-axial orientation versus bubble BOPP. A detail of material characterization can be found in the Supporting Information.

Prebreakdown Conduction Measurement System: A sinusoidal modulation signal was superimposed on the high voltage ramp and caused a capacitive current through the sample in addition to that caused by the high voltage ramp. A precision high-voltage oscilloscope probe measured the ramp plus the modulation signal applied to the sample and was used as a "reference". The reference signal was passed through a voltage-controlled amplifier (VCA), the gain of which was controlled by the output of a digital lock-in amplifier. The conditioned current signal from the sample and the gain-controlled reference signal were applied to a differential amplifier, the output of which fed the lock-in, the phase reference of which was set so that the output of the lock-in controlled the gain of the VCA so as to cancel the capacitive component of the signal through the sample. For a linear system, the cancellation of the sinusoidal capacitive current through the sample results in the cancellation of all capacitive currents through the sample. The remaining signal at the output of the differential amplifier represented the residual resistive current through the sample. The biggest advantage of this hardware cancellation was that it tracked the capacitive current in real time with a lock-in amplifier, and a better signal-to-noise ratio was obtained compared with post data processing. The real-time feedback system also provided the ability to measure nonlinear materials.

Probing of Density of States: In the prebreakdown conduction measurement, with the metalized film electrodes' Ohmic contact and the predominant band conduction happened at the high electric field, both major assumptions were fulfilled to use the SCLC model.[35] For a simplified transport model with unipolar carrier injection from an ideal ohmic contact free from thermal equalization, the application of the SCLC principle to the coupled transport and Poisson equations resulted in the following bulk density of trap states, measured in reference to the mobility edge of the conduction band, from the TD-SCLC spectra.[22,30,31] The shape of these experimentally determined SCLC curves reflected the increment of the space charge with respect to the shift of Fermi energy during the transient application of the high field.[22,31] The first and higher order derivatives of the temperature-modulated current density plots as a function of electric field could be employed to yield transport parameters such as the density of trap states.[35] The equation is given as

$$\frac{dn_s}{dE_f} = \frac{1}{k_B T}\frac{\varepsilon\varepsilon_0}{eL^2}\frac{2m-1}{m^2}(1+C) \tag{1}$$

with

$$C = \frac{B(2m-1)+B^2(3m-2)+d[\ln(1+B)]/d\ln U}{1+B(m-1)} \tag{2}$$

and

$$B = \frac{dm}{d\ln(U)}\frac{1}{m(m-1)(2m-1)} \tag{3}$$

where L is the sample thickness, U is the applied voltage, $m = d(\ln j)/d(\ln U)$, the slope of the log–log j-U plot. With the parameter determined from Equations (2) and (3), Equation (1) gives the density of state as a function of the applied field for each material. Arrhenius analysis of the TD-SCLC spectra was used to extract the activation energy as a function of U according to $E_a = -d(\ln j)/d(k_b T)^{-1}$ to correlate the electric field to the energy level of the traps which were being filled at.

DFT Computational Details and Models: DFT computations were performed using the Vienna ab initio simulation package.[36] Perdew–Burke–Ernzerhof (PBE) XC functional[37] and a plane-wave energy cutoff of 400 eV were used. Monkhorst-Pack k-point meshes of 4 × 1 × 4, 4 × 4 × 2, 1 × 1 × 4, and 1 × 1 × 1 were applied for crystal PP, PET, PS, and all amorphous structures, respectively (Figure S7, Supporting Information). The vdW-DF2 functional was adopted to improve the van der Waals interactions.[38] In addition, the electronic structure of crystal polymers was computed using the HSE06 functional.[39] While the electronic structure of amorphous phases was corrected at the hybrid DFT level, based on the relationship between the PBE and HSE06 results derived from 250 polymeric and molecular structures. Classical MD simulations were performed in the LAMMPS simulation package,[40] using the OPLS-AA force field[41] and a time-step of 1 fs.

Classical MD simulations were used to generate amorphous phases of isotactic PP, isotactic PS, and PET, including 1808, 2568, and 2260 atoms respectively. The following MD procedures were performed: 1) NVT (T = 600 K, 0.5 ns); 2) NPT (P = 1 atm, T = 600 K, 2 ns); 3) quench liquid to solid state from 600 to 300 K at NPT ensemble over 1 ns; 4) NPT (T = 300 K, 5 ns). The resulting densities of isotactic PP, isotactic PS, and PET are 0.85, 1.01, and 1.26 g cm^{-3} respectively, agreeing well with experimental values.[42]

Supporting Information

Supporting Information is available from the Wiley Online Library or from the author.

Acknowledgements

Z.L. and C.W. contributed equally to this work. This work was supported through a multidisciplinary university research initiative (MURI) grant (N00014-17-1-2656) and a capacitor program grant (N0014-19-1-2340), both from ONR. The authors would like to thank JoAnne Ronzello for assistance in the experimental setup.

Conflict of Interest

The authors declare no conflict of interest.

Data Availability Statement

The data that support the findings of this study are available from the corresponding author upon reasonable request.

Keywords

charge transport, conduction, electronic band structures, polymer dielectrics, prebreakdown

Received: October 10, 2023
Revised: January 6, 2024
Published online:

[1] M. S. Whittingham, *MRS Bull.* **2008**, *33*, 411.
[2] Q. Zhang, V. Bharti, X. Zhao, *Science* **1998**, *280*, 2101.
[3] Q. Chen, Y. Shen, S. Zhang, Q. Zhang, *Annu. Rev. Mater. Res.* **2015**, *45*, 433.
[4] W. J. Sarjeant, et al., in *Handbook of Low and High Dielectric Constant Materials and Their Applications*, Elsevier, Amsterdam **1999**.
[5] Y. Cao, P. C. Irwin, K. Younsi, *IEEE Trans. Dielectr. Electr. Insul.* **2004**, *11*, 797.
[6] U. Shinohara, *Memo of Hokkaido Univ.* **1936**, *3*, 157.
[7] I. D. L. Ball, *Proc. IEE-Part I: Gen.* **1951**, *98*, 84.
[8] A. Von Hippel, *J. Appl. Phys.* **1937**, *8*, 815.
[9] H. Fröhlich, *Nature* **1943**, *151*, 339.
[10] H. Zeller, *IEEE Trans. Electr. insul.* **1987**, 115.
[11] H. Li, D. Ai, L. Ren, B. Yao, Z. Han, Z. Shen, J. Wang, L.-Q. Chen, Q. Wang, *Adv. Mater.* **2019**, *31*, 1900875.
[12] M. Ieda, *IEEE Trans. Electr. Insul.* **1980**, *EI-15*, 206.
[13] V. Sharma, C. Wang, R. G. Lorenzini, R. Ma, Q. Zhu, D. W. Sinkovits, G. Pilania, A. R. Oganov, S. Kumar, G. A. Sotzing, S. A. Boggs, R. Ramprasad, *Nat. Commun.* **2014**, *5*, 4845.
[14] Y. Sun, S. Boggs, R. Ramprasad, *Appl. Phys. Lett.* **2012**, *101*, 132906.
[15] L. Chen, T. D. Huan, R. Ramprasad, *Sci. Rep.* **2017**, *7*, 6128.
[16] L. A. Dissado, J. C. Fothergill, *Electrical Degradation and Breakdown in Polymers*, IET, London **1992**.
[17] J. Ho, T. R. Jow, *IEEE Trans. Dielectr. Electr. Insul.* **2012**, *19*, 990.
[18] Y. Cao, S. Boggs, *Ann. Rep. Conf. Electr. Insul. Dielectr. Phenomena.* **2001**, 236.
[19] B. B. Sauer, P. Avakian, H. W. Starkweather, B. S Hsiao, *Macromolecules* **1990**, *23*, 5119.
[20] M. Li, S. Menon, J. P. Nibarger, G. N. Gibson, *Phys. Rev. Lett.* **1999**, *82*, 2394.
[21] G. Sessler, B. Hahn, D. Yoon, *J. Appl. Phys.* **1986**, *60*, 318.
[22] M. A. Lampert, R. B. Schilling, in *Semiconductors and Semimetals*, Elsevier, Amsterdam, **1970**.
[23] C. L. McBee, J. Kruger, *Phys. Sci.* **1971**, *230*, 194.
[24] J. O'Dwyer, *J. Electrochem. Soc.* **1969**, *116*, 239.
[25] S. Diaham, M.-L. Locatelli, *Appl. Phys. Lett.* **2012**, *101*, 242905.
[26] Z. Li, C. Xu, H. Uehara, S. A. Boggs, Y. Cao, *AIP Adv.* **2016**, *6*, 115025.
[27] C. Laurent, G. Teyssedre, S. Le Roy, F. Baudoin, *IEEE Trans. Dielectr. Electr. Insul.* **2013**, *20*, 357.
[28] F.-C. Chiu, *Adv. Mater. Sci. Eng.* **2014**, *2014*, 578168.
[29] D. Fabiani, G. Montanari, L. Dissado, *Solid Dielectrics (ICSD), 2010 10th IEEE International Conference on*, IEEE, Potsdam **2010**.
[30] F. Schauer, S. Nespurek, O. Zmeskal, *J. Phys. C: Solid State Phys.* **1986**, *19*, 7231.
[31] A. Rose, *Phys. Rev.* **1955**, *97*, 1538.
[32] M. Ieda, M. Nagao, M. Hikita, *IEEE Trans. Dielectr. Electr. Insul.* **1994**, *1*, 934.
[33] G. Natta, P. Pino, P. Corradini, F. Danusso, E. Mantica, G. Mazzanti, G. Moraglio, *J. Am. Chem. Soc.* **1955**, *77*, 1708.
[34] J. L. Nash, *Polym. Eng. Sci.* **1988**, *28*, 862.
[35] F. Schauer, S. Nešpůrek, H. Valerián, *J. Appl. Phys.* **1996**, *80*, 880.
[36] G. Kresse, J. G. K. Furthmuller, J. Furthmüller, *Phys. Rev. B* **1996**, *54*, 11169.
[37] J. P. Perdew, K. Burke, M. Ernzerhof, *Phys. Rev. Lett.* **1996**, *77*, 3865.
[38] M. Dion, H. Rydberg, E. Schröder, D. C. Langreth, B. Lundqvist, *Phys. Rev. Lett.* **2004**, *92*, 246401.
[39] J. Heyd, G. E. Scuseria, M. Ernzerhof, *J. Chem. Phys.* **2003**, *118*, 8207.
[40] S. Plimpton, *J Comput Phys.* **1995**, *117*, 1.
[41] M. J. Robertson, J. Tirado-Rives, W. L. Jorgensen, *J. Chem. Theory Comput.* **2015**, *11*, 3499.
[42] J. E. Mark, *Polymer Data Handbook*, Oxford University Press, New York **2009**.